Molecular Determinants of Topoisomerase I Poisoning by Lamellarins: Comparison with Camptothecin and Structure−Activity Relationships

Esther Marco,[†] William Laine,[‡] Christelle Tardy,[‡] Amélie Lansiaux,[‡] Masatomo Iwao,[§] Fumito Ishibashi,[§] Christian Bailly,*[,‡] and Federico Gago*[,†]

Departamento de Farmacología, Universidad de Alcalá, E-28871 Madrid, Spain, INSERM U-524 and Laboratoire de Pharmacologie Antitumorale du Centre Oscar Lambret, IRCL, Place de Verdun, F-59045 Lille, France, and Faculty of Engineering and Faculty of Fisheries, Nagasaki University, Nagasaki 852-8521, Japan

Received November 19, 2004

A series of lamellarin derivatives have been studied as topoisomerase I (Top1) inhibitors. Molecular models of the ternary complexes formed between the DNA-Top1 ensemble and lamellarin D (LMD) or camptothecin (CPT) fully intercalated into the duplex DNA have been built and studied by means of nanosecond molecular dynamics simulations in aqueous solution. Our results show that the 20-OH and 8-OH of LMD can participate in hydrogen-bonding interactions with the side chains of Glu356 and Asn722, respectively, the latter being consistent with the finding that CEM/C2 cells, which are resistant to CPT, are cross-resistant to LMD. Our models also account for the observation that LMD stabilizes Top1 cleavage at CG sites in addition to the TG sites observed for CPT and rationalize the structure−activity relationships within the series. The deleterious effect of replacing the 20-OH in LMD with a hydrogen was confirmed using a set of thermodynamic integration free energy simulations.

Introduction

Eukaryotic topoisomerase I (Top1) is the target for the anticancer drug camptothecin (CPT),[1] first isolated and identified from the bark of the Chinese yew tree, *Camptotheca acuminata* (for recent reviews, see refs 2−4). This pentacyclic alkaloid, however, was early shown to be clinically problematic because, in addition to its negligible water solubility, its active "ring-closed" α-hydroxylactone form (see the E-ring in Figure 1) is rapidly converted under physiological conditions to the "open" carboxylate form,[5,6] which is inactive and readily binds to human serum albumin,[7] making it inaccessible for cellular uptake.

Top1 mediates relaxation of supercoiled DNA by creating a transient single-strand break in the DNA duplex that originates from a transesterification reaction involving a nucleophilic attack by the active-site tyrosine (Tyr723) hydroxyl group on a DNA phosphodiester bond situated at the site of cleavage.[4] The resulting 3′-phosphotyrosine enzyme−DNA complex ("covalent binary complex") is then reversed, after DNA relaxation through strand passage, when the released 5′-OH of the nicked strand reattacks the phosphotyrosine intermediate in a second transesterification reaction. By binding the covalent 3′-phosphotyrosyl intermediate, Top1 inhibitors such as CPT specifically block religation of the DNA phosphodiester backbone and enzyme release, thus converting Top1 into a DNA-damaging agent that reduces cell viability.[8]

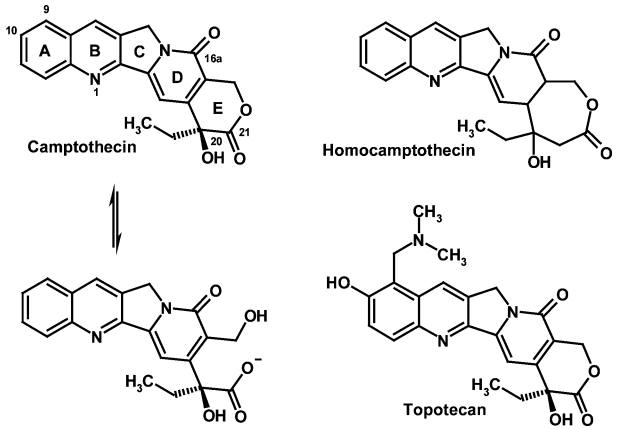

Figure 1. Chemical structures of camptothecin (open and closed forms), homocamptothecin, and topotecan. Ring positions relevant to the discussion have been numbered.

In an attempt to stabilize the closed lactone of CPT, a seven-member E-ring derivative was synthesized and named homocamptothecin (hCPT, Figure 1).[9,10] The β-hydroxylactone E-ring of hCPT is indeed considerably more stable in vitro,[11] while at the same time hCPT has been shown to inhibit Top1-mediated DNA relaxation with a potency comparable to that of CPT[9] and to give rise to novel Top1-mediated DNA breaks.[12] First-generation analogues of CPT, such as irinotecan and topotecan (Figure 1), which are water-soluble derivatives of CPT with an intact lactone ring, are already approved as anticancer agents in human therapy, and several second- (e.g., lurtotecan, rubitecan, and exatecan) and third-generation derivatives (e.g., diflomotecan) are well advanced into clinical trials. Nevertheless, identification of alternative molecular scaffolds endowed with similar properties is highly desirable, and this is facilitated by the availability of biochemical and cellular assays for testing Top1 activity.[13] One promising class

* To whom correspondence should be addressed. For C.B.: phone, (+33) 320 16 92 18; fax, (+33) 320 16 92 29; e-mail, bailly@lille.inserm.fr. For F.G.: phone, +34-918 854 514; fax, +34-918 854 591; e-mail, federico.gago@uah.es.

[†] Universidad de Alcalá.

[‡] INSERM U-524 and Laboratoire de Pharmacologie Antitumorale du Centre Oscar Lambret.

[§] Nagasaki University.

10.1021/jm049060w CCC: $30.25
Published on Web 05/03/2005

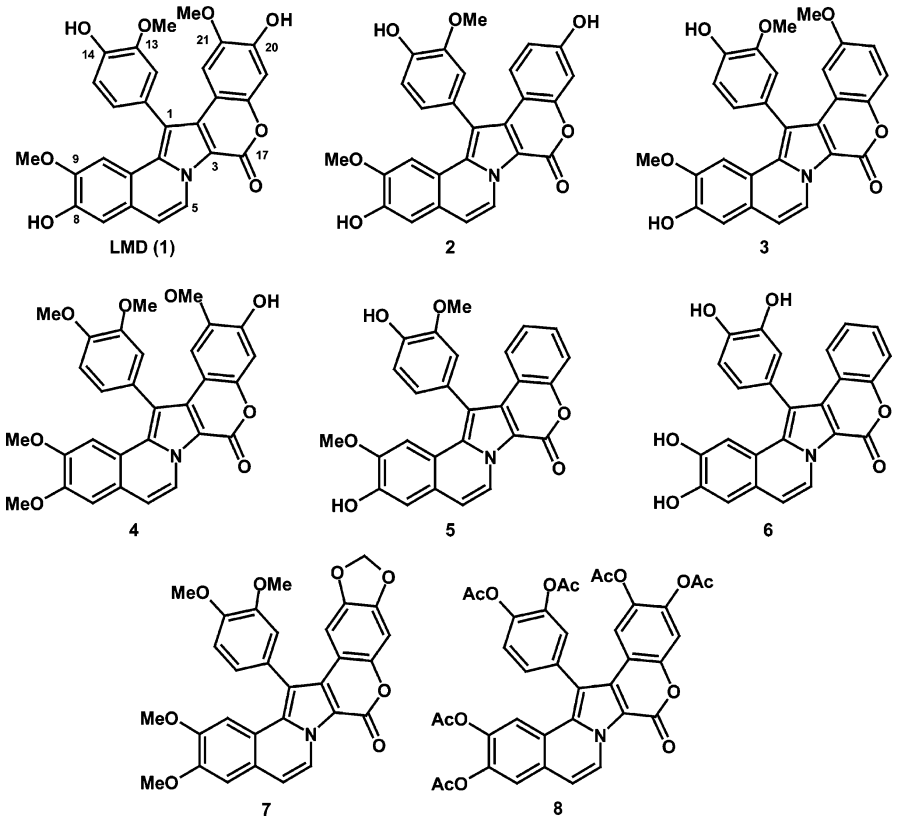

Figure 2. Chemical structures of the lamellarins studied. Ring positions relevant to the discussion have been numbered as in ref 20.

of Top1 inhibitors is that of the 6*H*-[1]benzopyrano-[4,3;4,5]pyrrolo[2,1-*a*]isoquinoline alkaloids known as lamellarins, of which about 30 representatives have been isolated from marine organisms so far.[14] Only four alkaloids, lamellarins A−D, were initially extracted from a prosobranch mollusk (*Lamellaria* sp.),[15] but later many closely related compounds were identified from several ascidian and sponge species. These molecules fall into three structural groups depending on whether the central pyrrole ring is fused or unfused (lamellarins O−R) to adjacent aromatic rings and on the presence between atoms 5 and 6 of the quinoline moiety of either a single (as in lamellarins I−L) or a double bond (as is the case for lamellarins D and M).[14] Lamellarin D (LMD, **1** in Figure 2), one of the most cytotoxic compounds in the series and not sensitive to P-glycoprotein-mediated drug efflux,[16] was recently found to promote DNA cleavage through the stabilization of Top1−DNA covalent complexes so that most, if not all, of its proapoptotic action is thought to arise from Top1 inhibition.[17] Elucidation of this mechanism of action provides useful guidelines for the development of progressible hits[18] targeted to the Top1−DNA cleavable complex. In this respect, triester and aminoacyl derivatives of LMD have already been selected for preclinical development.[19]

To further delineate the structure−activity relationships (SAR) in this promising chemical series, we report here our biochemical and biological in vitro evaluation of eight lamellarin derivatives (**1**−**8** in Figure 2) whose synthesis and cytotoxic potential against normal and tumor cells using a colony assay have been previously reported.[20] In addition, since no experimental structural information is available about the mode of binding of these compounds to the covalent Top1−DNA complex, we have used a variety of molecular modeling and simulation techniques to validate and refine a previously proposed binding mode for LMD to the DNA−Top1 complex[17] based on the X-ray crystal structure of a ternary complex between a human Top1 construct covalently attached to a DNA duplex with bound topotecan.[21] For comparison purposes, the same molecular dynamics (MD) protocol was applied to a similar complex containing CPT for which no such information is currently available. Finally, to support our model of the Top1−DNA cleavable complex stabilized by LMD, a quantitative estimation of the contribution to the free energy of binding of the crucial 20-OH group was obtained by means of a set of precise thermodynamic integration free energy simulations.

Results and Discussion

Topoisomerase I Inhibition. The effects of the lamellarin derivatives on Top1-mediated cleavage and relaxation of supercoiled plasmid DNA are shown in Figure 3. DNA was relaxed with Top1 in the absence or presence of the compounds, each tested at 5 and 20 μM. The DNA relaxation products were then resolved by gel electrophoresis on agarose gels containing ethidium bromide to stain the DNA. The plant alkaloid CPT, used as a positive control at 20 μM, was seen to strongly stabilize the cleaved complex with Top1. The intensity of the band corresponding to nicked DNA was amplified to a comparable extent in the presence of **1** (LMD) and **2**, indicating that these two compounds are also very effective at stabilizing DNA−Top1 covalent complexes. In this assay, at 5 μM practically no effect was observed

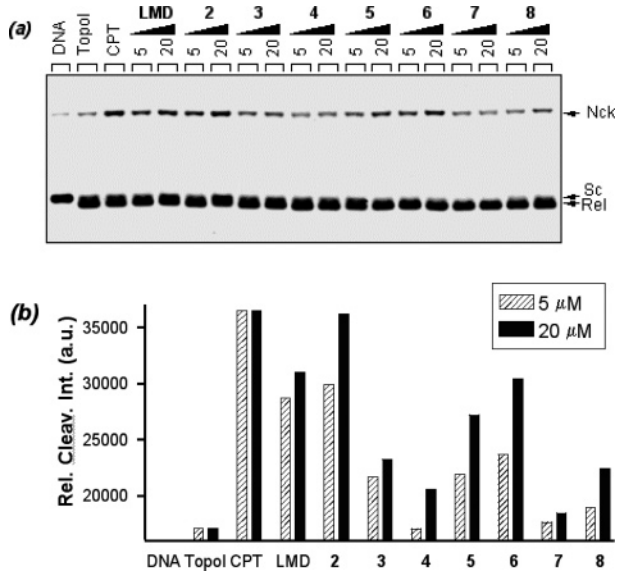

Figure 3. Effect of CPT (20 μM) and the different lamellarins on the relaxation of plasmid DNA by human topoisomerase I. (a) Native supercoiled pLAZ3 DNA (0.5 μg) (lane DNA) was incubated with 4 units of topoisomerase I in the absence (lane TopoI) or presence of drug at the indicated concentration (μM). Reactions were stopped with sodium dodecyl sulfate and treatment with proteinase K. DNA samples were separated by electrophoresis on 1% agarose gels containing ethidium (1 μg/mL) and then photographed under UV light: Nck, nicked; Rel, relaxed; Sc, supercoiled DNA. (b) Comparison of the extent of topoisomerase I-mediated DNA cleavage measured with CPT and LMD. The graph shows the formation of nicked DNA (form II, %) as a function of the drug concentration. Band intensities from three gels such as the one shown in (a) were compiled for the quantitative analysis.

with compounds **4**, **7**, and **8**, and only minor inhibitory activity was detected in the presence of **3**, **5**, and **6**.

A second assay, based on the cleavage of a radiolabeled DNA substrate by Top1, was used to further investigate the SAR. A 117-base-pair DNA restriction fragment uniquely end-labeled at the 3′ end was subjected to cleavage by Top1 in the presence of the different compounds, and the resulting DNA cleavage products were resolved on a sequencing-type polyacrylamide gel (Figure 4). This assay allows the detection of cleavage sites and their location in the sequence with nucleotide resolution, thus providing information on the selectivity of cleavage. Marked Top1 poisoning was detected for CPT as well as for **1** and **2**, whereas this effect was less pronounced for **3** and **5**, both lacking the 20-OH group. **6** and **8** showed greatly diminished activity, and virtually no cleavage was detected in the presence of **4** and **7**, both lacking the 8-OH. These results are therefore consistent with those obtained in the previous relaxation assay.

The presence of CPT stabilizes Top1-induced DNA breaks at nucleotide positions 26, 48, 81, and 107, all of them corresponding to T$^{\downarrow}$G sites separated by at least 20 base pairs. As previously discussed for LMD,[17] the cleavage pattern in the presence of **1** and **2** is slightly different: (i) the intensity of the nick promoted at site T$^{\downarrow}$G$_{81}$ is less intense than that induced by CPT, and (ii) an additional cleavage site at C$^{\downarrow}$G$_{73}$ that is not observed with CPT is clearly apparent. It must be noted, however, that the T$^{\downarrow}$G$_{81}$ and C$^{\downarrow}$G$_{73}$ sites are separated by only five base pairs, and this proximity could be the reason

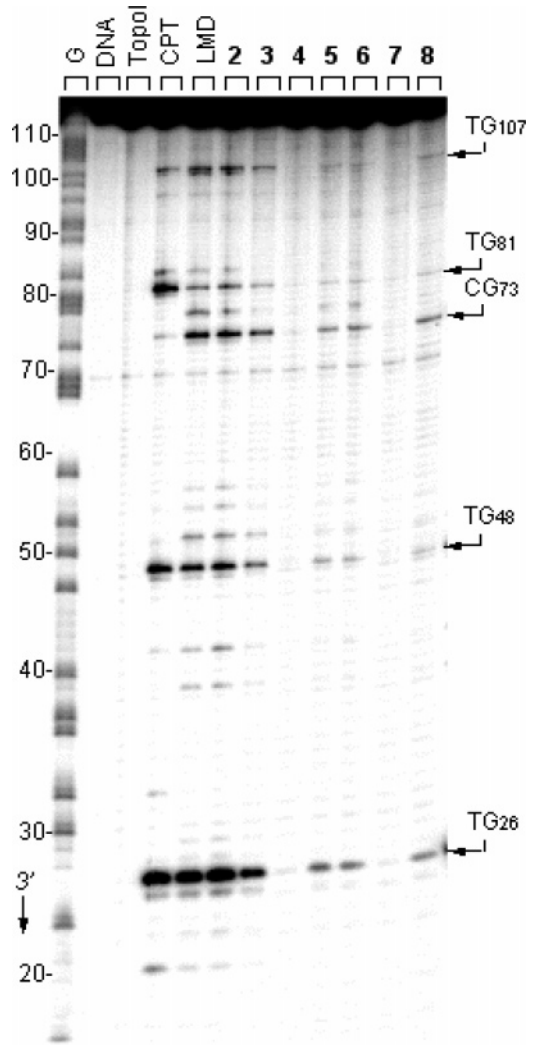

Figure 4. Cleavage of the 117-mer DNA restriction fragment by topoisomerase I (Top1) in the presence of the different compounds. In each case, the 3′-end labeled fragment (lane DNA) was incubated in the absence (lane TopoI) or presence of the test drug at 20 μM concentration. Camptothecin (CPT) was also used at 20 μM. Top1 cleavage reactions were analyzed on 8% denaturing polyacrylamide gels. Numbers at the side of the gels show the nucleotide positions, determined with reference to the guanine tracks labeled G. The nucleotide positions and sequences of the main cleavage sites are indicated.

accounting for the less efficient cleavage promoted by LMD at T$^{\downarrow}$G$_{81}$ relative to CPT. The same reasoning applies to the observation that another putative CG target step at position 41 (and therefore close to the T$^{\downarrow}$G$_{48}$ strong cleavage site) is spared. It is also noteworthy that in all DNA cleaved sites a T or an A is selected at position −2. In light of the structural evidence[21] and the binding model described below, this preference is due to the direct recognition of N3 of adenine or O2 of thymine in the DNA minor groove by the charged amino group of Lys532. This amino acid is strongly selecting against a guanine or a cytosine at position −2 (as, for example, at position CG$_{88}$), in excellent agreement with the known sequence preferences for Top1, both in the absence[22] and in the presence of bound drugs.[23] Likewise, the strong bias for a G at position +1 in the presence of CPT[23] appears to be also true for lamellarins.

Table 1. Cytotoxicity of Lamellarins and CPT (IC_{50})[a] on CEM and CEM/C2 Cells

	IC_{50},[a] nM		
compd	CEM	CEM/C2	RRI[b]
1	5 ± 2	720 ± 60	144
2	17 ± 4	2740 ± 680	164
3	520 ± 140	6250 ± 2110	12
4	3030 ± 2320	5550 ± 4670	2
5	2230 ± 10	11050 ± 2600	5
6	430 ± 30	950 ± 150	2
7	>100 000	>100 000	
8	1950 ± 1210	6930 ± 4860	4
CPT	0.84 ± 0.1	5385 ± 742	6400

[a] Drug concentration that inhibits cell growth by 50% after incubation in liquid medium for 72 h. Each drug concentration was tested in triplicate. IC_{50} values were measured using a cell proliferation assay (CellTiter 96, Promega). [b] The relative resistance index (RRI) is the ratio of the IC_{50} values measured on the CPT-resistant cell line to the IC_{50} values measured on the CPT-sensitive cell line.

Cytotoxicity and Structure−Activity Relationships. Two human cell lines, CEM and CEM/C2, were employed to evaluate the cytotoxic potential of the lamellarin derivatives and the role of Top1 inhibition in the apoptotic process. Human leukaemia CEM cells express an intact top1 gene encoding a fully functional Top1 enzyme, whereas CEM/C2 cells, which are resistant to CPT, express a mutated top1. The resistance of these cells to CPT has been attributed to a single Asn722 → Ser mutation adjacent to the active site Tyr723 residue of the human Top1 enzyme.[24] The antiproliferative activity of the lamellarins was evaluated by a tetrazolium-based assay, and the IC_{50} values and relative resistance index (RRI) were calculated for each compound (Table 1).

It can be seen that the cytotoxic potency of the compounds varies considerably depending on the presence and location of the free OH substituents on the lamellarin ring systems. On one hand, **1** (LMD) and **2** were, by far, the most cytotoxic molecules in the series, in agreement with previous findings.[20] We now find that this potent activity can be related to their capacity to inhibit Top1; the low IC_{50} value measured with **1**, in the low nanomolar range, is fully consistent with those recently reported for this compound against a panel of tumor cell lines.[17] On the other hand, the bulky methylenedioxy compound **7**, with no free OH groups, proved to be totally inactive in the Top1 assay and showed no signs of cytotoxicity even at high concentrations. Remarkably, the peracetylated **8** was quite cytotoxic despite its total inactivity against Top1, strongly suggesting that this compound might be acting as a prodrug that becomes active upon biotransformation. Interestingly, the micromolar IC_{50} values measured with Top1-inactive compounds **4**, **5**, and **8** on CEM cells are comparable to those determined with **2** on CEM/C2 cells. Similarly, the submicromolar IC_{50} values measured with the less active compounds **3** and **6** on CEM cells are roughly equivalent to that measured with **1** on CEM/C2 cells. Collectively, these results suggest that the gain in cytotoxicity observed from one series of compounds to another is most likely attributable to the Top1 inhibitory activity. It must be noted, however, that cell death occurs in vivo at much lower concentrations than those that are necessary for visualizing the enzymatic inhibitory mechanism in vitro.

A number of SAR observations can then be made:

(i) The presence of the 21-methoxy group has no significant impact on the inhibitory or cytotoxic activity; in fact, the RRI for **1** and **2** are very similar, thus reinforcing the idea of a major role for Top1 in the cytotoxic action of these compounds.

(ii) Deletion of the 20-OH group has a strong deleterious effect on the antiproliferative activity of these alkaloids. Lamellarin**3**, lacking this hydroxyl relative to **1**, is about 50 times less cytotoxic and is also less effective in the Top1-mediated DNA cleavage assay. The molecular basis for this result was probed computationally using a thermodynamic integration free energy simulation method (see below).

(iii) Replacing the 8-OH group with a 8-OCH_3 group, as in going from **1** to **4**, also considerably reduces the cytotoxic activity and suppresses the effect on Top1-mediated DNA cleavage. Thus, both OH groups, at positions 8 and 20 on **1** and **2**, are major determinants of the cytotoxic action.

(iv) The more hydrophilic tetrahydroxylated compound **6**, in which the 20-OH is missing, is fairly cytotoxic, but it has no effect on Top1 action, again in agreement with the idea that the 20-OH group is crucial for Top1 inhibition.

As indicated in Table 1, the cytotoxic activity of **1** is significantly reduced when the leukemia cell line expresses a mutated top1. This is also the case for the closely related analogue **2** lacking the 21-methoxy group on the benzopyrane ring. CEM/C2 cells are about 150 times less sensitive to **1** and **2** compared to the parental CEM cell line expressing a wild-type top1. For the other compounds in the series, **3**−**8**, the expression of a deficient Top1 enzyme only modestly reduces their cytotoxic action. Lamellarin **3**, which showed a considerably reduced inhibitory activity against Top1 relative to LMD, displays a cytotoxicity that is only scarcely dependent on Top1 activity (compare the RRI for **1** and **3** in Table 1) but is nevertheless greater than those of **4** and **5**, which are both totally inactive in the enzymatic assay. In general, an excellent correlation was found between the activity of the compounds determined at the molecular level with the purified Top1 enzyme and their cellular activity measured against the CEM and CEM/C2 pair of cell lines. The fact that the potent anti-Top1 activity of **1** and **2** is revealed at both the molecular and cellular levels suggests that neither cell uptake nor distribution is an issue with these molecules because they can apparently reach their intracellular target very effectively.

Docking of the Drugs into Their Respective Intercalation Sites. CPT. The automated docking program provided 11 clusters for bound CPT at the TpG intercalation step, the most populated one also being the first in the score list (56 occurrences and −13.0 kcal mol^{-1}). Remarkably, in this orientation the ring skeleton of CPT was practically superimposable (root-mean-square deviation of 0.3 Å) on that of topotecan as found in several X-ray crystal structures in which the latter drug is intercalated into the duplex DNA that is covalently bound to a trapped wild-type[21] or CPT-resistant (Asn722 → Ser and Phe361 → Ser) form[25] of human Top1.[26] In this orientation, the 20-OH donates to the side chain carboxylate of Asp533 the only drug−

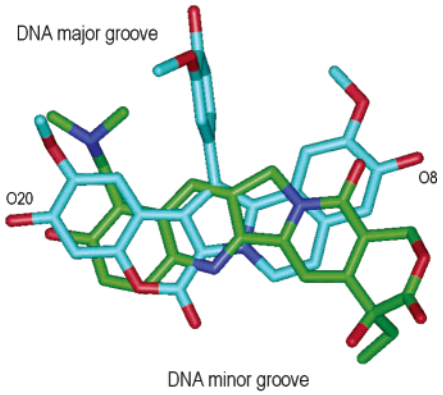

Figure 5. Superposition of CPT (C atoms in green) and LMD (C atoms in cyan) in the optimal solutions provided by the automated docking program. Note the position of the exocyclic ring of LMD in the major groove and the good alignment between oxygens at the left and right edges of both molecules.

protein hydrogen bond that is observed in these crystal structures. This reproducibility attests to the good performance of the docking program when challenged with a preconfigured binding site. It must be borne in mind that the precise atomic details of the interaction with CPT-like Top1 inhibitors were fully understood only when topotecan was cocrystallized with the "covalent binary complex" despite the previous existence of X-ray crystal structures of Top1 interacting both covalently and noncovalently with DNA.[27,28]

LMD. The same docking program provided six clusters for LMD, the most populated one ranking second in the score list by a negligible difference relative to the first (−9.30 vs −9.34 kcal mol^{-1} but 83 occurrences vs 4). This orientation (Figure 5) was chosen for one of the two initial conformers (see Materials and Methods) and was selected as representative of the mode of binding of LMD to the DNA-Top1 complex based on the following considerations:

(i) The C8 and C20 hydroxyl groups are at hydrogen-bonding distances from the side chains of Asn722 and Glu356, respectively, of Top1, and the keto group (O17) is facing the guanidinium group of Arg364. This is in consonance with the fact that this positively charged residue faces a region of LMD that gives rise to a negative molecular electrostatic potential (MEP) in the vicinity of the pyrane keto group (Figure 6), whereas the positive MEP region emanating from the isoquinoline ring points toward the negatively charged Asp533, also facing the DNA minor groove.

(ii) The planar heterocyclic ring system of the drug, which intercalates at the site of DNA cleavage and places the exocyclic phenyl ring in the major groove, is stabilized by stacking interactions with both the −1 (T−A) and +1 (G−C) base pairs of the bound oligonucleotide.

(iii) The exocyclic phenyl ring of LMD is rotated 180° relative to the conformation reported previously in an otherwise very similar proposal[17] so that the methoxy group at C13 is close to the 6-amino group of A'_{-1} in the major groove rather than to the 6-keto group of G_{+1}.

Since LMD was shown to bind to both TpG and CpG steps, two different oligonucleotides were considered for model construction and the same binding mode that was found for the TpG site was used for modeling the second complex (see Materials and Methods).

Comparison of the Top1−DNA−CPT and Topoisomerase I−DNA−LMD Complexes Obtained from the Molecular Dynamics Simulations. To assess the feasibility of the binding orientations found and to study the dynamic behavior of the proposed Top1−DNA−LMD and Top1−DNA−CPT molecular models, the three complexes were allowed to explore the conformational space by calculating MD trajectories in aqueous solution. MD computer simulations constitute a valuable means of developing models and interpreting diverse experimental data on the structure of DNA, proteins, and their mutual complexes in solution, with or without experimentally derived restraints.[29−31] Recent advances in force field parameters, simulation methodology, and computer power have made possible the simulation of reliable trajectories in terms of intermolecular forces and motions that give an independent account of experimentally observed behavior, including drug-induced DNA bending,[29,31] DNA−protein recognition,[30] and ligand−protein interactions.[32] For Top1, this type of approach has already shown its merit when trying to understand the molecular basis of CPT resistance brought about by the single Ala653 → Pro mutation in the linker domain due to a strong shift in the cleavage-religation equilibrium toward religation.[33]

The 725 snapshots from the last 1500 ps of each trajectory were analyzed in terms of distances and intermolecular energy components. Monitoring the progression of the root-mean-square deviations of the coordinates of the Cα atoms with respect to both the initial and average structures (Supporting Information, Figure S1) revealed a notably stable behavior in all cases, reflecting that the overall architectures of the macromolecular ensembles were preserved for the whole length of the simulations. Both drugs remained fully intercalated, giving rise to stacking interactions with the DNA bases and to a number of other stabilizing interactions with both the protein and the surrounding solvent that are described further below.

1. Top1−DNA−CPT Complex (CG−CPT). In the initial structure of the complex, only one direct hydrogen bond between the 20(*S*)-hydroxyl oxygen atom of CPT and one of the Asp533 carboxylate oxygens was observed that reproduced an identical interaction between topotecan and Top1 reported in the X-ray crystal structures.[21,25] Interestingly, this hydrogen bond has been proposed to exist for the lactone and the carboxylate forms of the drug, both of which could be placed into the electron density maps, with partial occupancies of ∼0.6 and ∼0.4, respectively. In the latter case, one of the 21-carboxylate oxygens is bridged to the phosphotyrosine (P-Tyr723) through a water molecule, and a second water molecule mediates a hydrogen bond between the new hydroxyl and the side chain amide group of Asn722 (this interaction is direct in PDB structure 1rr8). In the complexes with both the open and closed forms, the 10-OH of topotecan is also hydrogen-bonded to another water molecule.

Along our MD simulation with the closed form of CPT, two more direct interactions were detected: one between the 20-OH and the Nζ of Lys532 and another one between the E-ring carbonyl oxygen (O19) and a guanidinium nitrogen from the catalytic Arg488, whose side chain is found in a more extended conformation than

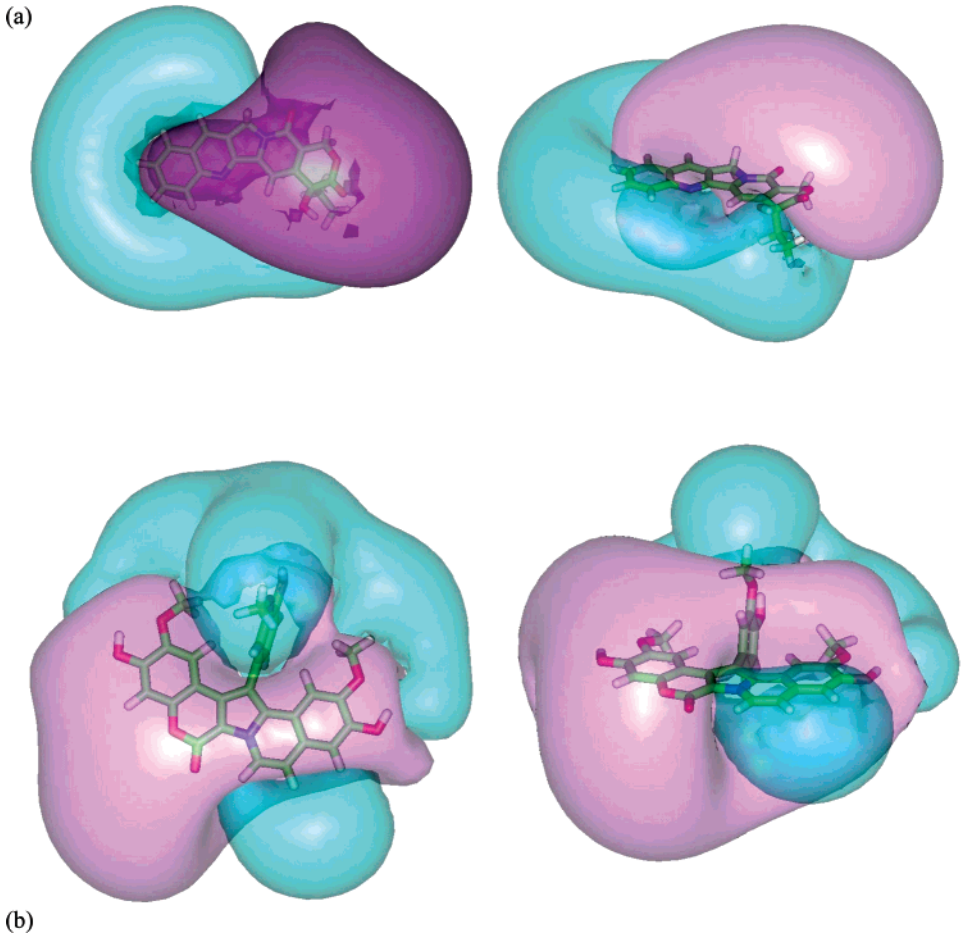

Figure 6. Top (left) and side (right) views of the molecular electrostatic potentials (MEP) calculated for (a) CPT and (b) LMD represented as two semitransparent contours surrounding a stick representation of each molecule. Negative (−0.05 to −2.26 kcal mol^{-1} for CPT and −0.05 to −4.04 kcal mol^{-1} for LMD) and positive MEP regions (0.05−1.67 kcal mol^{-1} for CPT and 0.05−7.47 kcal mol^{-1} for LMD) are in pink and cyan, respectively.

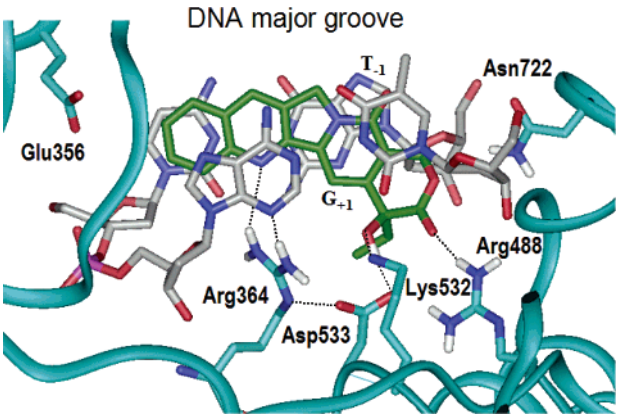

Figure 7. Schematic representation of the proposed binding mode for CPT in the Top1−DNA complex. Carbon atoms of CPT and DNA are in green and gray, respectively. The Cα trace of Top1 is displayed as a cyan ribbon, and only the side chains of amino acids relevant to the discussion are labeled and shown as sticks. Relevant hydrogen bonds are shown as dotted lines.

in the X-ray crystal structures (Figure 7). The rearrangement of these two side chains with respect to the crystallographic structures most likely reflects the obvious absence of the open form in our simulation (which is present in the crystal lattice) and slight positional differences brought about by the additional substituents on ring A of topotecan. Thus, the position of Nζ-Lys532 is determined by the carboxylate of CPT and by the O2 of T_{-1}, and this forces the side chain of Arg488 away through electrostatic repulsion. In common with the crystallographic structures, however, the guanidinium of Arg364, which is held in place with the aid of a buttressing interaction from the carboxylate of Asp533 (Figure 7), is facing the B-ring nitrogen of CPT. Moreover, hydrogen bonds between N1 of CPT and the NH1 of Arg364 appear to form and break during the simulation (Supporting Information, Figure S2). As a consequence, the average distance reported in Table 2 turns out to be slightly longer than that required for establishing a good hydrogen bond. Likewise, the lactone oxygen of CPT is close to the amide nitrogen of Asn722, but the distance is not short enough to allow the formation of a stable hydrogen bond. Again, in the crystallographic structures some uncertainties arise about this interaction due to the presence of a direct or water-mediated hydrogen bond between this amide and the hydroxyl generated upon E-ring opening in bound topotecan.

2. Top1−DNA−LMD Complexes (CG−LMD and TG−LMD). During the unrestrained MD simulation, the hydrogen bond initially observed in the CG−LMD complex between the pyrane keto group of LMD and the guanidinium group of Arg364 (Figure 8a) was maintained throughout (Table 2). On the other hand, the direct hydrogen bonding interactions between the 20-

Table 2. Intermolecular Hydrogen-Bonding Donor−Acceptor Distances (Mean ± Standard Deviation, Å) Observed in the Modeled Complexes Studied between Topoisomerase I Residues and Atoms of the Drug Intercalated at the Central CpG or TpG Step of the Duplex DNA

	lamellarin D			camptothecin
complex	CpG	TpG	complex	TpG
O20−OE1 Glu356[a]	3.4 ± 0.7	2.8 ± 0.3	O18−ND2 Asn722	3.6 ± 0.4
O17−NH1 Arg364	2.8 ± 0.1	2.8 ± 0.1	N1−NH1 Arg364	3.5 ± 0.3
O8−OD1 Asn722[a]	3.4 ± 0.4	3.6 ± 0.5	O20−NZ Lys532	3.2 ± 0.2
O8−ND2 Asn722[a]	3.6 ± 0.7	3.3 ± 0.5	O20−OD1 Asp533	2.7 ± 0.1
			O19−NH2 Arg488	2.8 ± 0.1
			H10−OE1 Glu356[b]	3.5 ± 0.4

[a] These direct interactions are often exchanged with similar water-mediated hydrogen bonds. [b] This distance is included for reference purposes only (see text for details).

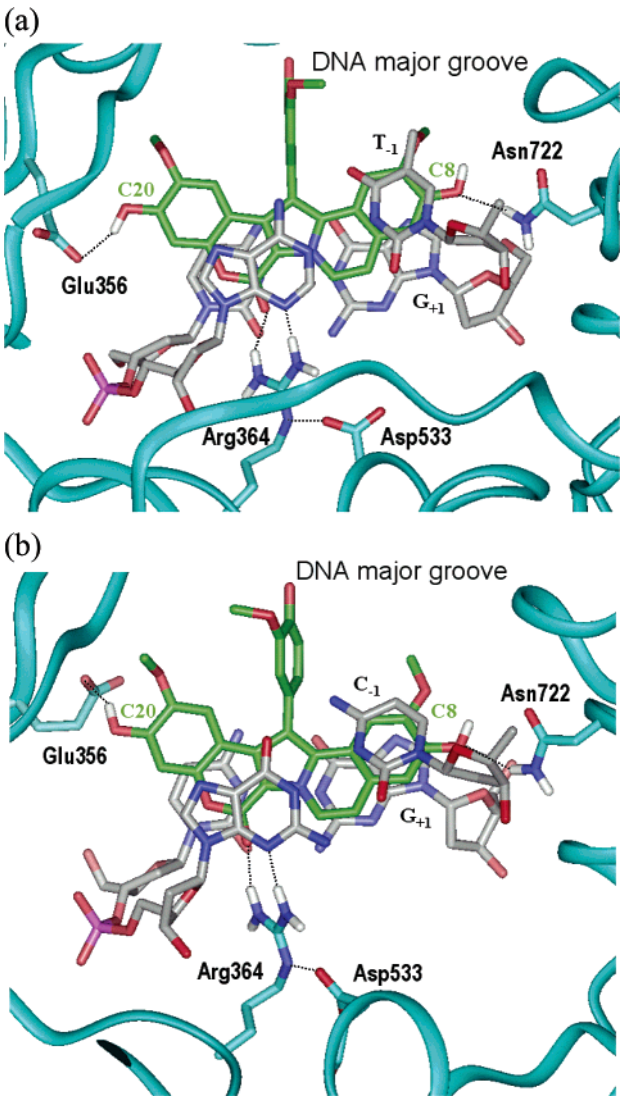

Figure 8. Schematic representation of the proposed binding site for LMD in the two Top1−DNA complexes studied containing (a) the TG olinucleotide and (b) the CG oligonucleotide. Carbon atoms of CPT and DNA are in green and gray, respectively. The Cα trace of Top1 is displayed as a cyan ribbon, and only the side chains of amino acids relevant to the discussion are labeled and shown as sticks. Relevant hydrogen bonds are shown as dotted lines.

OH oxygen and the Glu356 carboxylate oxygen and also between the 8-OH oxygen and the side chain amide nitrogen of Asn722 were often broken and re-formed during the entire simulation. Nonetheless, when these hydrogen bonds were ruptured, each of the hydrogen-bonding partners engaged in similar interactions with a common neighboring water molecule.

In the TG−LMD complex, the protein residues involved in interactions with LMD were the same although the atomic details were subtly different. Thus, the hydrogen bonds initially observed between the 20-OH group and Glu356, as well as those formed between the pyrane keto group and Arg364, were maintained throughout (Table 2). With respect to the Asn722 side chain amide, during the first 1300 ps the oxygen was continually engaged in a water-mediated hydrogen bond with the 8-OH of LMD whereas the nitrogen alternatively donated a hydrogen bond to either this same hydroxyl or neighboring water molecules. For the last 200 ps of simulation this interaction was fully water-mediated as described above for the CG−LMD complex (Figure 8b).

Energy Analysis of the Top1−DNA−CPT and Top1−DNA−LMD Complexes. The binding energy analysis of the Top1−DNA−CPT and Top1−DNA−LMD complexes (Table 3) reveals a predominance of van der Waals interactions involving the nucleic bases that make up the intercalation site and electrostatic interactions with some crucial protein residues. In the three cases studied, the most favorable and quantitatively more important interaction is with G_{+1}, although in the CG−LMD complex the magnitude of this van der Waals term is similar to that between LMD and the guanine complementary to C_{-1}. Remarkably, the interaction with T_{-1} is more favorable for CPT (by about 3 kcal mol^{-1}) than it is for LMD. On the other hand, both TpG and CpG sites provide equally good binding sites for LMD. The lack of detectable Top1-induced $C^{i}G$ sites in the presence of CPT could be explained by the steric clash that would arise between the exocyclic 4-amino group of C_{-1} and the sp^3 carbon in ring C. We can speculate that minor rearrangements in the docked orientation at the intercalation site must take place for the closely related hCPT due to the presence of a bulkier E-ring because this compound has been shown to stabilize cleavage at TpG sites as well.[12]

Arg488, Lys532, Asp533, Arg364, and Glu356 provide, in decreasing order of importance, electrostatic stabilization to CPT within the intercalation site. Despite the good hydrogen bond with the 20-OH, the magnitude of the electrostatic interaction with Asp533 is less than those with the positively charged residues because of the proximity between the negatively charged aspartate and the E-ring carbonyl oxygen of CPT (Figure 7). In contrast, although Glu356 is not involved in any direct hydrogen bond with CPT, the favorable electrostatic term arises from the interaction of this amino acid's carboxylate with the region of positive electrostatic potential surrounding C10 (Figure 6).

Table 3. Calculated van der Waals and Electrostatic Interaction Energies[a] between the Drugs and Both the DNA Bases Making Up the Intercalation Site and Crucial Top1 Residues in the Simulated CG−LMD, TG−LMD, and TG−CPT Complexes

lamellarin D						camptothecin		
	CpG			TpG			TpG	
	E_{vdW}	E_{ele}		E_{vdW}	E_{ele}		E_{vdW}	E_{ele}
C_{-1}	-8.8 ± 0.8	0.2 ± 0.2	T_{-1}	-8.5 ± 0.9	-0.2 ± 0.2	T_{-1}	-11.3 ± 1.1	0.7 ± 0.1
G'_{-1}	-13.2 ± 1.1	0.7 ± 0.2	A'_{-1}	-13.4 ± 0.6	1.2 ± 0.2	A'_{-1}	-11.0 ± 1.0	0.1 ± 0.2
G_{+1}	-12.7 ± 1.1	-0.5 ± 0.1	G_{+1}	-13.9 ± 1.2	-0.5 ± 0.4	G_{+1}	-13.8 ± 1.3	-0.3 ± 0.2
C'_{+1}	-10.7 ± 0.8	0.8 ± 0.2	C'_{+1}	-9.9 ± 1.8	0.8 ± 0.2	C'_{+1}	-6.3 ± 0.6	0.1 ± 0.3
Glu356	-1.5 ± 1.1	-1.2 ± 1.6	Glu356	-0.2 ± 0.4	-2.8 ± 1.4	Glu356	-1.0 ± 0.3	-0.5 ± 0.1
Arg364	0.1 ± 0.9	-4.4 ± 0.6	Arg364	-0.5 ± 0.1	-4.1 ± 0.5	Arg364	-3.9 ± 0.4	-1.1 ± 0.6
Asp533	-0.2 ± 0.1	0.4 ± 0.1	Asp533	-0.2 ± 0.1	0.4 ± 0.1	Arg488	0.0 ± 0.6	-3.8 ± 0.5
Asn722	-0.2 ± 0.5	-0.7 ± 0.4	Asn722	-0.9 ± 0.04	-0.7 ± 0.1	Lys532	-1.4 ± 0.3	-2.2 ± 0.6
						Asp533	-0.4 ± 1.2	-1.2 ± 0.9
						Asn722	-1.3 ± 0.4	0.0 ± 0.4

[a] These results are mean values ± standard deviation (kcal mol^{-1}) from snapshots taken every 100 ps from the last 1.4 ns of the molecular dynamics simulations.

Scheme 1. Thermodynamic Cycle Used To Estimate the Binding Free Energy Changes Involved When a Hydroxyl Group in LMD (**1**) Is Replaced with a Hydrogen (as in **3**) in the Free Drug in Solution (ΔG_3) and in Each Solvated Top1−DNA Complex (ΔG_4), Respectively

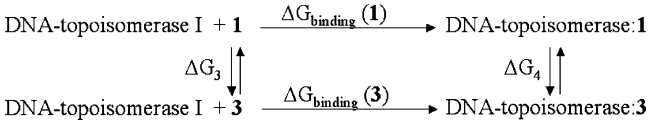

LMD appears to stack equally well on the G−C base pair at position +1 in both complexes, and the interaction with the base pair at position −1 is only slightly different, favoring the larger surface area of the C−G base pair over that of the T−A base pair. The electrostatic term is dominated by Arg364, which, as stated above, forms a good hydrogen bond with the carbonyl O17, followed by Glu356 and Asn722. The electrostatic interaction between LMD and the latter two residues is also favorable, but as explained above, it is often disrupted by intervening water molecules, hence the smaller energy values and the greater fluctuations.

Binding Free Energy Calculations. A rather dramatic decrease in activity is apparent upon the loss of the hydroxyl groups at positions 8 and 20 of the lamellarins' heteroaromatic ring. The rationale for the interaction between 8-OH and Asn722 has already been discussed and is substantiated, albeit indirectly, by the results obtained with the mutant Asn722 → Ser Top1 enzyme. On the other hand, to the best of our knowledge, Glu356 has not been described as important for the binding of any Top1 inhibitor despite the fact that its side chain is found in proximity to the C10-hydroxyl present in the X-ray Top1−DNA−topotecan complexes. Since our simulations consistently showed the 20-OH of LMD to be engaged in a direct or water-mediated hydrogen bond with the carboxylate of this residue, we decided to test whether the loss of this interaction might account for the decrease in activity observed in going from compound **1** (LMD) to **3**. To this end, a thermodynamic cycle (Scheme 1) was devised that would allow us to use statistical mechanical information generated during a set of MD simulations to calculate the difference in binding free energy between these two molecules. This method is commonly applied in drug design and is most successful when one tries to predict the effect of changing a simple group into another within a congeneric series.[34,35]

The free energy difference associated with conversion of **1** to **3** in aqueous solution (Figure 9) was 18.5 kcal mol^{-1}, virtually the same value that was obtained from the independent reverse conversion of **3** to **1** (−18.8 kcal mol^{-1}). For the corresponding mutations in the Top1−DNA−inhibitor complexes, the average free energy changes for the forward and reverse simulations were 21.3 ± 0.05 kcal mol^{-1} in the CG complex and 21.6 ± 0.08 kcal mol^{-1} in the TG complex. The binding of **3** to the CG and TG Top1−DNA complexes was then calculated to be disfavored by 2.6 and 2.9 kcal mol^{-1}, respectively, relative to the binding of **1**, in very good agreement with the 2.7 kcal mol^{-1} calculated from their respective IC_{50} values (see Materials and Methods). Even though this comparison must be considered very cautiously because cytotoxicity stems from both pharmacokinetic and pharmacodynamic parameters, this result lends further credence to the proposed binding mode. In fact, it is interesting that incorporation of a hydroxyl at the C10 position of CPT, as in topotecan (Figure 1) and other simpler analogues,[36] results in greatly improved Top1 inhibitory activity. According to our models, this OH is positionally equivalent to the 20-OH of LMD (Figure 5).

Comparison of Lamellarin D with Camptothecin as Topoisomerase I Inhibitors. LMD and CPT appear to make use of distinct sets of interactions to stabilize their unique binding modes at the intercalation sites in their respective Top1−DNA complexes and block the religation phase of the enzyme's catalytic cycle. Most noteworthy, the concave and convex sides of each molecule are found in different grooves of the DNA molecule (Figure 5), most likely as a result of (i) their distinct MEPs (Figure 6), (ii) the positioning of hydrogen bond acceptor and donor atoms in their polycyclic ring systems, and (iii) the compulsory location of the bulky exocyclic phenyl ring of lamellarin derivatives in the major groove (Figure 8). This finding should provide a cautionary note to researchers using other docking and modeling approaches based simply on molecular similarity because these can be sometimes misleading, especially in the absence of 3D structural information about the receptor binding site. Our results strongly suggest that C10 and C16a of CPT are positionally equivalent to C20 and C8 in lamellarins and also that oxygen atoms attached to these positions provide good

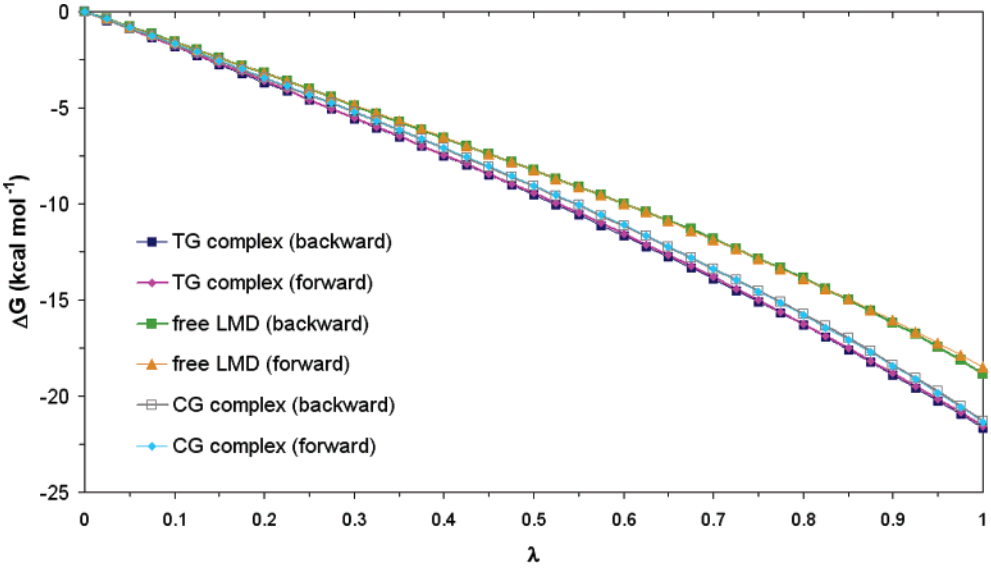

Figure 9. Cumulative free energy changes during the thermodynamic integration simulations (forward and reverse) of LMD both free and in the complexes with the CG- and TG-containing oligonucleotides.

anchoring points for stabilizing the cleavable complex through interactions with the side chains of Glu356 and Asn722. The crucial role of the latter residue is highlighted by the acquisition of resistance to both CPT and LMD in CEM/C2 cells harboring the Asn722 → Ser mutation in their Top1, which can be explained by the inability of the shorter side chain of Ser ($-CH_2-OH$) to establish the interactions described above for the side chain of Asn ($-CH_2-CO-NH_2$) at position 722. With regard to Glu356, its putative importance for LMD binding has been ascertained by means of thermodynamic integration simulations. Its actual role in the binding of CPT may have been obscured by the repositioning of its carboxylate in the complexes with topotecan possibly because of the simultaneous presence in this compound of a positively charged amine at position 9 of ring A (Figure 1).

Conclusions

Lamellarins provide a novel chemotype for Top1 inhibitors. We recently demonstrated that LMD (**1**), the lead compound in the series, functions as a potent Top1 inhibitor, and a preliminary molecular model of the enzyme−DNA−drug complex was proposed.[17] In the present work, this model has been refined and its feasibility has been extensively assessed by means of MD simulations in an attempt to account for the differences in activity observed for several close analogues. The experimental data indicate that the C8 and C20 hydroxyl groups in the lamellarin series studied are major determinants of both Top1 cleavable complex stabilization and cytotoxicity, thus reinforcing the idea that Top1 is a major player in the antitumor action of these compounds. The modeling results provide structural support to this structure−activity information, which can now be used to advantage in the design of novel analogues endowed with improved pharmacological properties.

The distinct MEP distributions calculated for CPT and LMD provide a rationale for their respective binding modes, as found by the automated docking program, and additionally suggest a possible mechanism of electrostatic steering into a common binding site within the cleavable complex. At least for lamellarins, entrance must take place from the major groove side of the DNA molecule because of the presence of the bulky exocyclic ring in this location and the simultaneous occupancy of the minor groove in the Top1−DNA binary complex by Asp533 in α-helix 13 (core subdomain III) and Arg364 in the loop segment between β-strands 6 and 7 (core subdomain I).[27]

Our MD simulation results support the feasibility of the proposed docking orientations and also unveil the critical role that water-mediated contacts and hydrogen bonding play in the affinity and efficacy of these potent anticancer drugs. In the case of LMD, additional endorsement of the proposed binding mode was provided by the good quantitative agreement that was obtained between the experimentally measured differences in inhibitory activity and the calculated differences in binding free energies using a very accurate thermodynamic integration method. Nonetheless, the IC_{50} ratio can be taken only as a rough approximation of differences in Top1 inhibition because the possibility that other cell killing mechanisms are simultaneously at play for these compounds cannot be ruled out.

The parallel study with CPT also provides some insight into the finding of the open form of the α-hydroxylactone ring of topotecan in the X-ray crystal structures solved to date. The lack of Top1 inhibitory activity of the carboxylate forms of both CPT[4] and hCPT[11] can be easily accounted for by considering the strongly negative MEPs associated with the free carboxylate forms (Supporting Information, Figure S3). On one hand, binding to the DNA polyanion would be disfavored on electrostatic grounds, and on the other hand, the intercalation process would have to overcome the repulsion between the free carboxylate of the drug and the facing Asp533 carboxylate in the minor groove. Since the open form is actually found in the binding site, its presence is strongly suggestive of in situ formation, which can be catalyzed under physiological conditions by the hydrogen-bonding network discussed above for CPT, and subsequent stabilization by a rearrangement

of Top1 side chains. In this regard, a certain level of general acid−base catalysis exerted by the cleavable complex toward E-ring opening has already been suggested.[12]

The structural (dis)similarities between CPT and LMD bound to the enzyme−DNA interface are of major interest to further explore the chemical environment around these two molecular frameworks. A goal that immediately comes to mind is to try and design novel LMD/CPT hybrid structures that could lead to innovative Top1-directed drugs. Beyond these medicinal chemistry aspects, the present work also provides interesting mechanistic clues to better understand the different cleavage profiles generated by CPT and LMD. Thus, Top1-mediated DNA cleavage at CG or TG sites is shown to depend on both the nature of the drug employed and the context in which the target sequence is embedded.

We hope that our contribution to a better understanding of the mechanism of Top1 poisoning by CPT and lamellarins will be beneficial for the ongoing development of some of these derivatives as effective anticancer agents.

Material and Methods

Drugs. The synthesis of the lamellarins studied here has been reported previously.[20] CPT was purchased from Sigma Chemical Co. The drugs were first dissolved in DMSO. Drug stock solutions (5 mM) were kept at −20 °C and were freshly diluted with water to the desired concentration immediately prior to use.

DNA Relaxation Experiments. Recombinant Top1 protein was produced and purified from baculovirus-infected Sf9 cells.[37] Supercoiled pLAZ3 DNA (0.5 μg) was incubated with 4 units of human Top1 at 37 °C for 1 h in relaxation buffer (50 mM Tris, pH 7.8, 50 mM KCl, 10 mM MgCl2, 1 mM dithiothreitol, 1 mM EDTA) in the presence of varying concentrations of the drug under study. Reactions were terminated by adding SDS to 0.25% and proteinase K to 250 μg/mL. DNA samples were then added to the electrophoresis dye mixture (3 mL) and electrophoresed at room temperature for 2 h at 120 V in 1% agarose gels containing ethidium bromide (1 mg/mL). After electrophoresis, gels were washed and photographed under UV light.[38]

Purification of the DNA Restriction Fragment and Radiolabeling. The 117-base-pair DNA fragment was prepared by 3′-[^{32}P]-end labeling of the *Eco*RI-*Pvu*II double digest of the pBS plasmid using α-[^{32}P]-dATP (Amersham, 3000 Ci/mmol) and AMV reverse transcriptase (Roche). The labeled digestion products were separated on a 6% polyacrylamide gel under nondenaturing conditions in TBE buffer (89 mM Tris-borate, pH 8.3, 1 mM EDTA). After autoradiography, the requisite band of DNA was excised, crushed, and soaked in water overnight at 37 °C. This suspension was filtered through a Millipore 0.22 μm filter, and the DNA was precipitated with ethanol. Following washing with 70% ethanol and vacuum-drying of the precipitate, the labeled DNA was resuspended in 10 mM Tris adjusted to pH 7.0 containing 10 mM NaCl.

Sequencing of Top1-Mediated DNA Cleavage Sites. Each reaction mixture contained 2 μL of 3′-end [^{32}P]-labeled DNA (∼1μM), 5 μL of water, 2 μL of 10× Top1 buffer, and 10 μL of drug solution at the desired concentration (1−50 μM). After 10 min of incubation to ensure equilibration, the reaction was initiated by addition of 2 μL (20 units) of calf thymus Top1. Samples were incubated for 45 min at 37 °C prior to adding SDS to 0.25% and proteinase K to 250 μg/mL to dissociate the drug−DNA−Top1 cleavable complexes. The DNA was precipitated with ethanol and then resuspended in 5 μL of formamide−TBE loading buffer, denatured at 90 °C for 4 min, and then chilled in ice for 4 min prior to loading onto the sequencing gel. DNA cleavage products were resolved by polyacrylamide (8%) gel electrophoresis under denaturing conditions (8 M urea). After electrophoresis, gels were soaked in 10% acetic acid for 10 min, transferred to Whatman 3MM paper, and dried under vacuum at 80 °C. A Molecular Dynamics 425E PhosphorImager was used to collect data. Baseline-corrected scans were analyzed by integrating all the densities between two selected boundaries using ImageQuant version 3.3 software.

Cell Cultures and Growth Inhibition Assay. Human CEM and CEMC2 leukemia cells were obtained from the American Tissue Culture Collection. The leukemia cells were grown at 37 °C in a humidified atmosphere containing 5% CO_2 in RPMI 1640 medium, supplemented with 10% fetal bovine serum, glutamine (2 mM), penicillin (100 IU/mL), and streptomycin (100 mg/mL). The cytotoxicity of the drug was assessed using a cell proliferation assay developed by Promega (CellTiter 96 AQ_{ueous} one solution cell proliferation assay). Briefly, 2×10^4 exponentially growing cells were seeded in 96-well microculture plates with various drug concentrations in a volume of 100 μL. After 72 h of incubation at 37 °C, 20 μL of the tetrazolium dye solution were added to each well and the samples were incubated for a further 3 h at 37 °C. Plates were analyzed on a Labsystems Multiskan MS (type 352) reader at 492 nm.

Building, Refinement, and Molecular Dynamics of the Protein−DNA−Inhibitor Complexes. The crystal structure of human Top1 covalently linked to double-stranded DNA with bound topotecan, at 2.10 Å resolution (PDB code: 1k4t),[21] was used as a template to model the drug-free covalent complexes between Top1 and two different DNA 15-mers. The sequences of these two oligonucleotides were taken from the 117-base-pair DNA restriction fragment used in the Top1-mediated DNA cleavage assays, and the drug intercalation site was centered on the $C^{\downarrow}G_{73}$ and $T^{\downarrow}G_{25}$ steps sites induced by LMD and/or CPT. Electrostatic-potential-derived charges for the drug molecules were obtained with the RESP methodology.[39] Two conformations of LMD differing in the orientation of the exocyclic phenyl ring (Figure 2) were input to the Lamarckian genetic algorithm implemented in AutoDock 3.0 to dock LMD within the intercalation site at the 5′-TpG step by randomly changing the overall orientation of the molecule as well as the torsion angles involving the methoxy groups. Default settings were used except for number of runs, population size, and maximum number of energy evaluations, which were fixed at 100, 50 and 250 000, respectively. Rapid intra- and intermolecular energy evaluation of each configuration was achieved by precalculating in a three-dimensional grid surrounding the protein−DNA complex (0.375 Å spacing) the affinity potentials for the carbon, oxygen, nitrogen, and hydrogen atoms present in LMD and CPT. Complexes representative of the most populated solutions were then refined using the second-generation AMBER force field[40] and 2000 steps of steepest descent energy minimization of only those atoms belonging to the bound drug and the replaced nucleobases. This procedure allowed readjustment of covalent bonds and van der Waals contacts without changing the overall conformation of the protein−DNA complex. The Top1−DNA−LMD and Top1−DNA−CPT complexes were then neutralized by addition of 12 sodium ions[41] that were placed in electrostatically favored positions and immersed in rectangular boxes each containing about 16 000 TIP3P water molecules[42] that extended 8 Å away from any solute atom. The cutoff distance for the nonbonded interactions was 9 Å, and periodic boundary conditions were applied. Electrostatic interactions were represented using the smooth particle mesh Ewald method with a grid spacing of ∼1 Å. Molecular dynamics (MD) simulations at 300 K and 1 atm were then run for 1.5 ns using the SANDER module in AMBER 8.[43] The coupling constants for the temperature and pressure baths were 1.0 and 0.2 ps, respectively. SHAKE[44] was applied to all bonds involving hydrogens, and an integration step of 2 fs was used throughout. The nonbonded pair list was updated every 10 steps. The simulation protocol was essentially as described,[29,30] involving a series of progressive

energy minimizations followed by a 10 ps heating phase and a 100 ps equilibration period during which distances involving hydrogen bonds between LMD and Glu356 and Asn722 were reinforced by means of an upper-bound harmonic restraining function with a force constant of 20 kcal mol^{-1} $Å^{-2}$. These restraints were removed during the following 1400 ps of data collection. System coordinates were saved every 2 ps for further analysis. For comparative purposes and validation of the protocol, the complex formed between CPT and the same oligodeoxynucleotide−Top1 covalent structure (in which the central CpG step was replaced by TpG) was simulated under identical conditions except that no restraints were initially applied.

Binding Free Energy Calculations. To further assess the feasibility of the proposed binding mode, we attempted to provide a quantitative estimation of the differences in binding free energy between compounds **1** (LMD) and **3**. To this end, the MD thermodynamic integration (TI) method and the "window growth" approach, as implemented in AMBER 6,[45] were used. Compound **1** was "mutated" into **3** and vice versa (Scheme 1), both free in aqueous solution (each immersed in a rectangular box containing 520 water molecules) and in a solvated Top1−DNA−inhibitor complex. Because of the computational overburden, the latter simulations for the bound inhibitors were carried out by adding a spherical cap of ~2100 TIP3P water molecules of radius 35 Å centered on the LMD molecule and including only the ligand, water molecules, and the core and C-terminal domains of the enzyme. The OH → H (forward) and H → OH (backward) "mutations" took place over a total of 41 "windows", each consisting of 5 ps of equilibration and 5 ps of data collection for averaging. SHAKE was used for all bonds, and the integration time step was 1 fs. Both bonded and nonbonded intramolecular energy contributions were included in the evaluation of the free energy differences, as recommended.[46] The nonbonded cutoff was 11.0, and the pair list was updated every 25 steps. A dielectric constant of 1 was used, and the temperature was kept at 300 K by use of the Berendsen algorithm with separate solute−solvent and solvent−solvent couplings. Water molecules, bound ligand, and protein side chains were free to move, whereas the protein Cα atoms as well as the DNA were fixed at their starting locations although they were included in the determination of the forces. The backward perturbation started from the end-point of the forward perturbation after a further equilibration of 500 or 100 ps, respectively, for the free or complexed **1** (LMD) and **3**. The relative free energy differences were then calculated as

$$\Delta\Delta G_{\text{binding}} = \Delta G_{\text{binding}}(\mathbf{3}) - \Delta G_{\text{binding}}(\mathbf{1}) = \Delta G_4 - \Delta G_3$$

and the experimental values were approximated from the differences in concentrations of each compound, giving rise to 50% inhibition of cell proliferation (IC_{50}) according to the expression

$$\Delta\Delta G_{\text{binding}} = -\text{RT} \ln \frac{IC_{50}(\mathbf{3})}{IC_{50}(\mathbf{1})}$$

Analysis of the Molecular Dynamics Trajectories and Electrostatic Energy Calculations. Three-dimensional structures and trajectories were visually inspected using the computer graphics program InsightII.[47] Root-mean-square deviations from the initial structures, interatomic distances, and distribution functions were monitored using the CARNAL module in AMBER. Finite difference solutions to the linearized Poisson−Boltzmann equation, as implemented in the DelPhi module (version 2.5) of Insight II, were used to calculate MEPs and electrostatic free energies. For MEP calculations on CPT and LMD, cubic grids with a resolution of 1.0 Å were centered on each molecule, and the atomic charges were distributed onto the grid points. AMBER charges and radii were used. Solvent-accessible surfaces, calculated with a spherical probe with a radius of 1.4 Å, defined the solute boundaries, and a minimum separation of 10 Å was left between any solute atom and the borders of the box. The potentials at the grid points delimiting the box were calculated analytically by treating each charge atom as a Debye−Hückel sphere. The interior of both the protein and the ligand was considered a low-dielectric medium ($\epsilon = 4$), whereas the surrounding solvent was treated as a high-dielectric medium ($\epsilon = 80$) with an ionic strength of 0.145 M. Intermolecular van der Waals energies for individual residues were calculated with the ANAL module, whereas the solvent-corrected residue-based electrostatic interaction energies were calculated with DelPhi, following the procedure described in detail elsewhere.[48,49]

All calculations were performed on the SGI R10000 Power Challenge at Alcalá University Computer Center, on the SGI R14000 Origin 3800 at CIEMAT (Madrid) and locally on SGI R5000 O2 workstations.

Addendum. After this paper was submitted, an article was published in this same journal reporting[50] the X-ray crystal structures of the human Top1−DNA complex bound with the lactone form of camptothecin (at 3.0 Å resolution) and representative members of the indenoisoquinoline and indolocarbazole classes of Top1 poisons. In agreement with our proposal, the superposition of these three ternary complexes reveals (i) the common presence of a hydrogen-bond acceptor on the minor groove side of the drug molecules (in the case of CPT, between the pyridine N1 atom and the Nϵ of Arg364), (ii) the presence of substituents on the major groove side, (iii) important contacts with amino acid residues Asn352 and Glu356, and also (iv) that the base-stacking interactions between drug molecules and the cleaved strand side of the DNA duplex are not spatially conserved.

Acknowledgment. E.M. enjoys a research fellowship from Junta de Comunidades de Castilla−La Mancha. This work was supported by research grants from the Ligue Nationale Contre le Cancer (Comité du Nord) and the Institut de Recherches sur le Cancer de Lille (IRCL) to C.B. and from the Spanish CICYT (Grant SAF2003-7219-C02), Pharma-Mar (Colmenar Viejo, Madrid), and the National Foundation for Cancer Research to F.G.. We thank the University of Alcalá Computing Centre and the CIEMAT (Madrid) for generous allowances of computer time on their SGI servers.

Supporting Information Available: Three additional figures reporting the time evolution of the root-mean-square deviations (rmsd) of the complexes, the time evolution of the distance between N1 of CPT and NH1 of Arg364 in the Top1−DNA−CPT complex, and the MEP calculated for the open form of CPT. This material is available free of charge via the Internet at http://pubs.acs.org.

References

(1) Hsiang, Y. H.; Hertzberg, R.; Hecht, S.; Liu, L. F. Camptothecin induces protein-linked DNA breaks via mammalian DNA topoisomerase I. *J. Biol. Chem*. **1985**, *260*, 14873−14878.
(2) Kim, D. K.; Lee, N. Recent advances in topoisomerase I-targeting agents, camptothecin analogues. *Mini-Rev. Med. Chem*. **2002**, *2*, 611−619.
(3) Oberlies, N. H.; Kroll, D. J. Camptothecin and taxol: historic achievements in natural products research. *J. Nat. Prod*. **2004**, *67*, 129−135.
(4) Thomas, C. J.; Rahier, N. J.; Hecht, S. M. Camptothecin: current perspectives. *Bioorg. Med. Chem.* **2004**, *12*, 1585−1604.
(5) Mi, Z.; Burke, T. G. Differential interactions of camptothecin lactone and carboxylate forms with human blood components. *Biochemistry* **1994**, *33*, 10325−10336.
(6) Fassberg, J.; Stella, V. J. A kinetic and mechanistic study of the hydrolysis of camptothecin and some analogues. *J. Pharm. Sci*. **1992**, *81*, 676−684.
(7) Burke, T. G.; Mi, Z. Preferential binding of the carboxylate form of camptothecin by human serum albumin. *Anal. Biochem*. **1993**, *212*, 285−287.
(8) Pourquier, P.; Pommier, Y. Topoisomerase I-mediated DNA damage. *Adv. Cancer Res*. **2001**, *80*, 189−216.
(9) Lavergne, O.; Lesueur-Ginot, L.; Plá-Rodas, F.; Bigg, D. C. H. BN 80245: An E-ring modified camptothecin with potent antiproliferative and topoisomerase I inhibitory activities. *Bioorg. Med. Chem. Lett*. **1997**, *7*, 2235−2238.

(10) Bailly C. Homocamptothecins: potent topoisomerase I inhibitors and promising anticancer drugs. *Crit. Rev. Oncol. Hematol*. **2003**, *45*, 91−108.
(11) Laco, G. S.; Du, W.; Kohlhagen, G.; Sayer, J. M.; Jerina, D. M.; Burke, T. G.; Curran, D. P.; Pommier, Y. Analysis of human topoisomerase I inhibition and interaction with the cleavage site +1 deoxyguanosine, via in vitro experiments and molecular modeling studies. *Bioorg. Med. Chem*. **2004**, *12*, 5225−5235.
(12) Bailly, C.; Lansiaux, A.; Dassonneville, L.; Demarquay, D.; Coulomb, H.; Huchet, M.; Lavergne, O.; Bigg, D. C. H. Homocamptothecin, an E-ring modified camptothecin analog, generates new topoisomerase I-mediated DNA breaks. *Biochemistry* **1999**, *38*, 15556−15563.
(13) Meng, L. H.; Liao, Z. Y.; Pommier, Y. Non-camptothecin DNA topoisomerase I inhibitors in cancer therapy. *Curr. Top. Med. Chem*. **2003**, *3*, 305−320.
(14) Bailly, C. Lamellarins, from A to Z: a family of anticancer marine pyrrole alkaloids. *Curr. Med Chem.: Anti-Cancer Agents* **2004**, *4*, 363−378.
(15) Andersen, R. J.; Faulkner, D. J.; Cun-heng, H.; Van Duyne, G. D.; Clardy, J. Metabolites of the marine prosobranch mollusc *Lamellaria* sp. *J. Am. Chem. Soc*. **1985**, *107*, 5492−5495.
(16) Vanhuyse, M.; Kluza, J.; Tardy, C.; Otero, G.; Cuevas, C.; Bailly, C.; Lansiaux, A. Lamellarin D: A novel pro-apoptotic agent from marine origin insensitive to P-glycoprotein-mediated drug efflux. *Cancer Lett*. **2005**, *221*, 165−175.
(17) Facompré, M.; Tardy, C.; Bal-Mayeu, C.; Colson, P.; Pérez, C.; Manzanares, I.; Cuevas, C.; Bailly, C. Lamellarin D: a novel potent inhibitor of topoisomerase I. *Cancer Res*. **2003**, *63*, 7392−7399.
(18) Valler, M. J.; Green, D. Diversity screening versus focussed screening in drug discovery. *Drug Discovery Today*. **2000**, *5*, 286−293.
(19) Tardy, C.; Facompré, M.; Laine M.; Baldeyrou, B.; García-Grávalos, D.; Francesch, A.; Mateo, C.; Pastor, A.; Jiménez, J. A.; Manzanares, I.; Cuevas, C.; Bailly, C. Topoisomerase I-mediated DNA cleavage as a guide to the development of antitumor agents derived from the marine alkaloid lamellarin D: Triester derivatives incorporating amino acid residues. *Bioorg. Med. Chem*. **2004**, *12*, 1697−1712.
(20) Ishibashi, F.; Tanabe, S.; Oda, T.; Iwao, M. Synthesis and structure−activity relationship study of lamellarin derivatives. *J. Nat. Prod*. **2002**, *65*, 500−504.
(21) Staker, B. L.; Hjerrild, K.; Feese, M. D.; Behnke, C. A.; Burgin, A. B., Jr.; Stewart, L. The mechanism of topoisomerase I poisoning by a camptothecin analog. *Proc. Natl. Acad. Sci. U.S.A.* **2002**, *99*, 15387−15392.
(22) Been, M. D.; Burgess, R. R.; Champoux, J. J. Nucleotide sequence preference at rat liver and wheat germ type 1 DNA topoisomerase breakage sites in duplex SV40 DNA. *Nucleic Acids Res*. **1984**, *12*, 3097−3114.
(23) Jaxel, C.; Capranico, G.; Kerrigan, D.; Kohn, K. W.; Pommier, Y. Effect of local DNA sequence on topoisomerase I cleavage in the presence or absence of camptothecin. *J. Biol. Chem*. **1991**, *266*, 20418−20423.
(24) Fujimori, A.; Harker, W. G.; Kohlhagen, G.; Hoki, Y.; Pommier, Y. Mutation at the catalytic site of topoisomerase I in CEM/C2, a human leukemia cell line resistant to camptothecin. *Cancer Res*. **1995**, *55*, 1339−1346.
(25) Chrencik, J. E.; Staker, B. L.; Burgin, A. B.; Pourquier, P.; Pommier, Y.; Lance, S.; Redinbo, M. R. Mechanisms of camptothecin resistance by human topoisomerase I mutations. *J. Mol. Biol*. **2004**, *339*, 773−784.
(26) PDB entries 1k4t, 1rr8, and 1rrj, respectively.
(27) Redinbo, M. R.; Stewart, L.; Kuhn, P.; Champoux, J. J.; Hol, W. G. J. Crystal structures of human topoisomerase I in covalent and noncovalent complexes with DNA. *Science* **1998**, *279*, 1504−1513.
(28) Redinbo, M. R.; Stewart, L.; Champoux, J. J.; Hol, W. G. Structural flexibility in human topoisomerase I revealed in multiple non-isomorphous crystal structures. *J. Mol. Biol.* **1999**, *292*, 685−696.
(29) García-Nieto, R.; Manzanares, I.; Cuevas, C.; Gago, F. Bending of DNA upon binding of ecteinascidin 743 and phthalascidin 650 studied by unrestrained molecular dynamics simulations. *J. Am. Chem. Soc*. **2000**, *122*, 7172−7182.
(30) Marco, E.; García-Nieto, R.; Gago, F. Assessment by molecular dynamics simulations of the structural determinants of DNA-binding specificity for transcription factor Sp1. *J. Mol. Biol*. **2003**, *328*, 9−32.
(31) Marco, E.; García-Nieto, R.; Mendieta, J.; Manzanares, I.; Cuevas, C.; Gago, F. A 3·(ET743)−DNA complex that both resembles an RNA−DNA hybrid and mimics zinc finger-induced DNA structural distortions. *J. Med. Chem*. **2002**, *45*, 871−880.
(32) Marco, E.; Martín-Santamaría, S.; Cuevas, C.; Gago, F. Structural basis for the binding of didemnins to human elongation factor eEF1A and rationale for the potent antitumor activity of these marine natural products. *J. Med. Chem*. **2004**, *47*, 4439−4452.
(33) Fiorani, P.; Bruselles, A.; Falconi, M.; Chillemi, G.; Desideri, A.; Benedetti, P. Single mutation in the linker domain confers protein flexibility and camptothecin resistance to human topoisomerase I. *J. Biol. Chem*. **2003**, *278*, 43268−43275.
(34) Pearlman, D. A.; Charifson, P. S. Are free energy calculations useful in practice? A comparison with rapid scoring functions for the p38 MAP kinase protein system. *J. Med. Chem*. **2001**, *44*, 3417−3423.
(35) de la Fuente, J. A.; Manzanaro, S.; Martín, M. J.; de Quesada, T. G.; Reymundo, I., Luengo, S. M.; Gago, F. Synthesis, activity, and molecular modeling studies of novel human aldose reductase inhibitors based on a marine natural product. *J. Med. Chem*. **2003**, *46*, 5208−5221.
(36) Laco, G. S.; Collins, J. R.; Luke, B. T.; Kroth, H.; Sayer, J. M.; Jerina, D. M.; Pommier, Y. Human topoisomerase I inhibition: docking camptothecin and derivatives into a structure-based active site model. *Biochemistry* **2002**, *41*, 1428−1435.
(37) Rossi, F.; Labourier, E.; Forné, T.; Divita, G.; Derancourt, J.; Riou, J. F.; Antoine, E.; Cathala, G.; Brunel, C.; Tazi, J. Specific phosphorylation of SR proteins by mammalian DNA topoisomerase I. *Nature* **1996**, *381*, 80−82.
(38) Bailly, C. DNA relaxation and cleavage assays to study topoisomerase I inhibitors. *Methods Enzymol*. **2001**, *340*, 610−623.
(39) Cieplak, P.; Cornell, W. D.; Bayly, C. I.; Kollman, P. A. Application of the multimolecule and multiconformational RESP methodology to biopolymers: charge derivation for DNA, RNA and proteins. *J. Comput. Chem*. **1995**, *16*, 1357−1377.
(40) Cornell, W. D.; Cieplak, P.; Bayly, C. I.; Gould, I. R.; Merz, K. M.; Ferguson, D. M.; Spellmeyer, D. C.; Fox, T.; Caldwell, J. W.; Kollman, P. A. A second generation force field for the simulation of proteins, nucleic acids, and organic molecules. *J. Am. Chem. Soc*. **1995**, *117*, 5179−5197.
(41) Åqvist, J. Ion−water interaction potentials derived from free energy perturbation simulations. *J. Phys. Chem*. **1990**, *94*, 8021−8024.
(42) Jorgensen, W. L.; Chandrasekhar, J.; Madura, J. D. Comparison of simple potential functions for simulating liquid water. *J. Chem. Phys*. **1983**, *79*, 926−935.
(43) URL: http://amber.scripps.edu/doc8/.
(44) Ryckaert, J. P.; Ciccoti, G.; Berendsen, H. J. C. Numerical integration of the Cartesian equations of motion of a system with constraints: molecular dynamics of *n*-alkanes. *J. Comput. Phys*. **1977**, *23*, 327−341.
(45) URL: http://amber.scripps.edu/doc6/.
(46) Pearlmann, D. A. Determining the contributions of constraints in free energy calculations: development, characterization, and recommendations. *J. Chem. Phys*. **1993**, *98*, 8946−8957.
(47) *Insight II*, version 98.0; Molecular Simulations Inc. (9685 Scranton Road, San Diego, CA 92121-2777), 1998.
(48) Gallego, J.; Ortiz, A. R.; de Pascual-Teresa, B.; Gago, F. Structure−affinity relationships for the binding of actinomycin D to DNA. *J. Comput.-Aided Mol. Des*. **1997**, *11*, 114−128.
(49) Pérez, C.; Ortiz, A. R.; Pastor, M.; Gago, F. Comparative binding energy analysis of HIV-1 protease inhibitors: incorporation of solvent effects and validation as a powerful tool in receptor-based drug design. *J. Med. Chem*. **1998**, *41*, 836−852.
(50) Staker, B. L.; Feese, M. D.; Cushman, M.; Pommier, Y.; Zembower, D.; Stewart, L.; Burgin, A. B. Structures of three classes of anticancer agents bound to the human topoisomerase I−DNA covalent complex. *J. Med. Chem*. **2005**, *48*, 2336−2345.

JM049060W